Highly crystalline $LiCu_XFe_{1-X}PO_4$ nanoparticles synthesized by high temperature thermal decomposition: a morphological and electrical transport study

2016 J. Phys. D: Appl. Phys. 49 335302

(http://iopscience.iop.org/0022-3727/49/33/335302)

IOP Publishing Journal of Physics D: Applied Physics
J. Phys. D: Appl. Phys. **49** (2016) 335302 (10pp) doi:10.1088/0022-3727/49/33/335302

Highly crystalline $LiCu_xFe_{1-x}PO_4$ nanoparticles synthesized by high temperature thermal decomposition: a morphological and electrical transport study

P Martinez[1,2], F Ruiz[1], J Curiale[1,2], M Vasquez Mansilla[1], R D Zysler[1,2], L Dada[3], M S Moreno[1,2], L Rodríguez[1], D Fregenal[1], G Bernardi[1] and E Lima Jr[1]

[1] CNEA, CONICET, Centro Atómico Bariloche, Avenida Bustillo 9500, 8400 S. C. de Bariloche, Río Negro, Argentina
[2] Instituto Balseiro, Universidad Nacional de Cuyo—Comisión Nacional de Energía Atómica, Avenida Bustillo 9500, 8400 S. C. de Bariloche, Río Negro, Argentina
[3] Universidad Nacional de Salta, CP4400, SAL, Argentina

E-mail: lima@cab.cnea.gov.ar

Received 27 March 2016, revised 7 June 2016
Accepted for publication 9 June 2016
Published 25 July 2016

Abstract

In this work, we report the morphological and electrical characterization of highly crystalline $LiCu_xFe_{1-x}PO_4$ nanoparticles synthesized via the high-temperature (380 °C) thermal decomposition of organometallic precursors. The mean diameter of the studied nanoparticles was 30–40 nm. The Cu/Fe relations of 0, 0.001 and 0.042 for the three studied samples were obtained via particle-induced x-ray emission spectroscopy. Crystallographic and morphological studies were performed using x-ray diffraction, transmission electron microscopy and high-resolution transmission electron microscopy techniques. We investigated the effects of incorporating copper on the electric transport properties of this highly crystalline nanometric system using impedance spectroscopy and DC transport techniques. The experimental evidence allowed us to conclude that in the frequency range $f < 1$ kHz the transport is dominated by the diffusion of Li and the presence of Cu atoms in the systems hinders this transport mechanism, despite the high crystallinity of the system.

Keywords: nanoparticles, impedance spectroscopy, li-ion batteries

(Some figures may appear in colour only in the online journal)

1. Introduction

The properties of nanoparticles with a diameter of less than 50 nm are related to their preparation method and thermal history [1]. This link between the synthesis method and the physical/chemical properties is closely related to the crystallinity of the nanoparticles and the density of defects. Concerning diffusion, these two points compete and lead to a non-trivial dependence [2, 3]: an increase in the density of the defect centers leads to different diffusion coefficient behavior. On the one hand, diffusion through vacancies increases, while on the other hand, interstitial diffusion tends to decrease.

Diffusion in nanometric materials for energy storage is a subject of strong technological interest, especially when the focus is on cathode materials for Li-ion batteries.

The high-temperature decomposition of organometallic precursors is a synthesis procedure that is widely used to produce highly crystalline nanoparticles [4] with complete control of the morphology and composition of the material. It is a very interesting method for the production of highly crystalline cathode materials for Li-ion batteries at the nanoscale; in

fact, Jiang *et al* [5] synthesized $LiFePO_4$ nanoparticles as a widely used cathode material. Studying the transport and Li diffusion in nanoparticles prepared using the thermal decomposition method is very interesting for understanding the effects of nanoscale on them.

Since the first report on the capabilities of $LiFePO_4$ as a material for cathodes in Li batteries [6], this material has aroused enormous interest, with a huge number of published papers in the basic and applied fields. Some of the properties discovered regarding the performance of this compound for applications revealed several advantages with respect to other cathodes, such as, safety, thermal stability, high stability for a large number of cycles, high operating voltage, and low cost, among others [7, 8].

Despite the number of studies on this material and the fact that $LiFePO_4$ is already being used as a cathode material in commercial Li-ion batteries, there are still many open questions to answer in order to improve and predict their performance [9]. Most of the questions that the scientific and technological community is focused on relate to the electric transport properties of the whole system, including the simultaneous electronic and ionic (Li diffusion) contributions.

It is known that the morphology of the $LiFePO_4$ at the nanoscale (<100 nm) plays an important role in its performance as a cathode material in Li-ion batteries [10]. The diffusion of Li ions is a fundamental parameter to take into account to establish a strategy to tune or improve $LiFePO_4$ performance. In this range of sizes, the increase of the surface/volume ratio as the nanoparticle size is reduced is expected to increase Li^+ diffusion through the olivine structure. Nevertheless, it is also expected that with decreasing size there will more defect centers, which will hinder the diffusion of Li^+ along the [0 1 0] direction. The competition between these two mechanisms means that there is an optimal size for diffusion [11]. The number of defect centers and the dependence of diffusion on size at the nanoscale are dependent on the crystallinity of the particles and, consequently, on the preparation method. Therefore, it is very important to understand the electrical transport mechanisms, especially for nanoscaled particles (<100 nm) and systems with doping ions or a carbon coating.

$LiFePO_4$ has an electronic conductivity of the order of 10^{-9}–10^{-10} S cm^{-1}, which is lower than that for other typical cathode materials [12, 13]. In this case, the origin of this intrinsic low electronic conductivity is related to the formation of a small magnetic polaron due to the doping of the d-hole in the Fe^{3+} site [14, 15]. Regarding the Li diffusion in $LiFePO_4$, it is a slow and unidirectional process that takes place specifically in the [0 1 0] crystallographic direction [15, 16]. The calculated diffusion coefficient for bulk systems varies from 10^{-13} to 10^{-16} cm^2 s^{-1}, depending on the amount of lithium [17]. For nanoscale amorphous material, diffusion coefficients of around 10^{-10} cm^2 s^{-1} were reported [18]. One strategy to improve the electronic conductivity of $LiFePO_4$ cathodes is so-called *carbon coating*, where the surface of the material is coated with conductor carbon. This strategy is used commercially nowadays, and it also improves the specific capacity, rate performance and some other characteristics of the cathodes and batteries. Nevertheless, the effects of carbon coating on the electrochemical properties of $LiFePO_4$ depend on the uniformity of the structure, morphology and composition [19]. Another route for improving the electrical conductivity of $LiFePO_4$ is ionic substitution with isovalent or aliovalent ions [20], which also improves the Li^+ diffusion and lattice stability of the system [7]. As was previously shown, the disorder produced by the doping modifies the crystal structure and increases the lithium mobility [21]. Despite the use of the strategies already pointed out, it is necessary to make a strong effort to improve the performance of cathodes based on $LiFePO_4$, and specifically to improve the transport properties.

Impedance spectroscopy (IS) has been widely used to study the electrical properties of $LiFePO_4$ and other cathodes materials [9, 17, 18, 22, 24]. One of the main reasons for this is that this technique allows us to determine several important parameters related to electric transport properties, such as different characteristic times, the associated energy barriers and the diffusion coefficient of Li^+ ions [17, 18].

In this work, we synthesized highly crystalline $LiCu_xFe_{1-x}PO_4$ nanoparticles with a mean diameter size in the range of 30–40 nm and different amounts of Cu ($X = 0$, 0.001 and 0.042). Their composition was analyzed via particle-induced x-ray emission (PIXE) and infrared spectroscopy. The morphology and crystallinity of the nanoparticles were studied by means of bright/dark field transmission electron microscopy (TEM), high-resolution TEM (HRTEM) and x-ray diffraction (XRD). We also present a thorough study and modeling of the AC and DC electric transport properties, which were mainly carried out using impedance spectroscopy. These studies allow us to attempt a deep understanding of transport phenomena in $LiFePO_4$ nanoparticles with a diameter of less than 40 nm and the effect of Cu incorporation at the nanoscale.

2. Experimental

$LiCu_xFe_{1-x}PO_4$ nanoparticles with 0, 0.5 and 6 at.% of Cu were prepared using the high-temperature (380 °C) thermal decomposition method, in a similar way to Jiang *et al* [5]. In this case, the precursors used were Li^+ acetylacetonate (Li(acac)), Cu^{2+} acetylacetonate ($Cu(acac)_2$), Fe^{3+} acetylacetonate ($Fe(acac)_3$) and ammonium phosphate dibasic ($(NH_4)_2HPO_4$). The solvents used were oleic acid ($C_{18}H_{34}O_2$) and oleylamine ($C_{18}H_{37}N$). During the synthesis, the amount of Cu in the sample was controlled by the stoichiometric addition of the Cu^{2+} precursor at the expense of Fe^{3+}. After the reaction (120 min at reflux condition—380 °C), nanoparticles were precipitated by the addition of ethanol to the solution. This action was carried out at room temperature with the amount of ethanol:precursor solution set at 8 : 1 and the mixture was then precipitated by centrifugation for 30 min at 14 000 rpm. The precipitated powder was washed with acetone in an ultrasound bath for 10 min. Finally, the washed solution was centrifuged again in order to obtain the 'as-made' sample. As expected from the synthesis procedure, the as-made samples were coated with a monolayer of oleic acid/oleylamine,

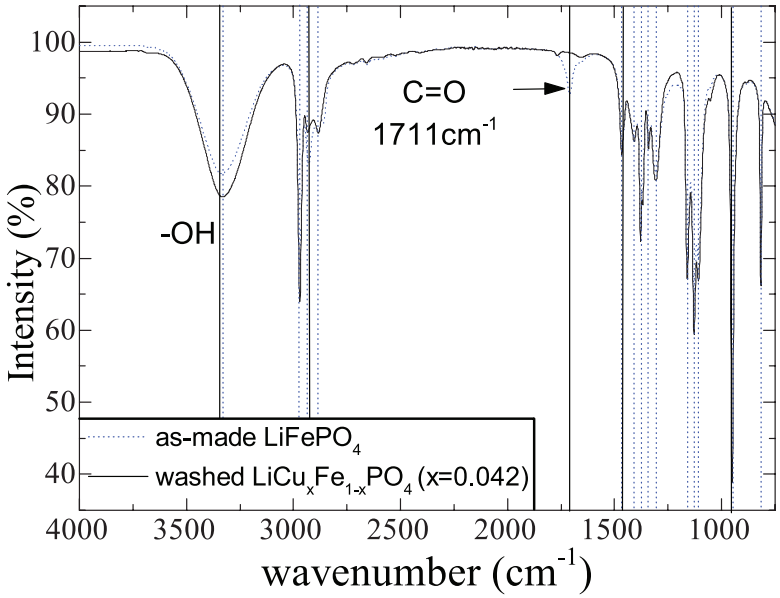

Figure 1. FTIR spectra of as-made $LiCu_xFe_{1-x}PO_4$ ($X = 0$) nanoparticles with an organic layer and (*fat-free*) washed $LiCu_xFe_{1-x}PO_4$ ($X = 0.042$) nanoparticles, both in an isopropyl alcohol suspension. The dotted vertical lines are the peaks associated with the alcohol and the solid vertical lines are the peaks associated with the oleic acid, where the C=O characteristic peak is emphasized.

making them easily dispersible in organic solvents because of their strongly hydrophobic character. This organic layer can be removed by acetone and an ultrasound bath (10 min) at 40 °C. This procedure was repeated several times until the nanoparticles were no longer dispersed in hexane and these samples were labeled *fat-free* samples and used in the transport measurements.

The Fourier transform infrared (FTIR) spectra were obtained using PerkinElmer 'spectrum two' equipment with a universal ATR optical system and the samples were dispersed in isopropyl alcohol with similar concentrations of nanoparticles.

The amount of Cu incorporated into the $LiCu_xFe_{1-x}PO_4$ nanoparticles was characterized using PIXE spectroscopy carried out with 2 MeV H^+ in a NEC 5SDH 1.7 MV tandem accelerator and a NEC RC43 end station. The PIXE spectra of three samples, conditioned as pellets, were collected with and without a 102 μm mylar filter and analyzed using GUPIX software [23].

The diffraction patterns were obtained in a Philips PW1700 diffractometer using Cu Kα radiation ($\lambda = 0.154\,186$ nm) and a graphite monochromator. The samples for the XRD experiments were prepared by dispersing the as-made powder on ground glass.

The TEM experiments were carried out with a FEI TECNAI G2 that worked at 200 kV and was equipped with a field emission gun. The TEM specimens were prepared by diluting a nanoparticle in chloroform and dropping it on a copper grid.

The samples for the transport measurements were prepared by washing the nanoparticles as previously discussed, and then these *fat-free* samples were uniaxially pressed with 8 tons in a hydraulic press. After that, we obtained cylindrical pellets with a diameter of 7 mm and a typical thickness of 200 μm. Electrical contacts were made on each pellet face using silver paste. DC measurements of voltage versus current (IV curves) were performed at room temperature using a Keithley 4200-SCS Parameter Analyzer with a two-terminal configuration. These measurements were performed from -20 V to 20 V with steps of 0.1 V in a characteristic total time of 1 min. Impedance spectroscopy was also measured at room temperature in the same samples used for the DC characterization. To make these measurements we used an Autolab PGSTAT30 potentiostat at the frequency range (10 mHz–1 kHz) and an Agilent 4294A Precision Impedance Analyzer for the (40 Hz–110 MHz) interval. Both sets of equipment were operated without bias voltage and with oscillator amplitudes of 0.3 V and 1 V for the potentiostat and the impedance analyzer, respectively. The impedance, defined as $Z = Z' + jZ''$, was normalized by its geometrical factor, as previously discussed.

3. Results and discussion

Figure 1 shows the FTIR spectra of as-made $LiFePO_4$ nanoparticles with an organic layer and (*fat-free*) washed $LiCu_XFe_{1-X}PO_4$ ($X = 0.042$) nanoparticles, both dispersed in isopropyl alcohol, as representative of all systems. The dotted vertical lines are the peaks associated with the alcohol and the solid vertical lines are the peaks associated with the oleic acid. The characteristic peak of the C=O in the oleic acid is emphasized (1711 cm^{-1}), between the two peaks associated with the phosphate group present in all the spectra. This peak is clearly observed for the as-made nanoparticles, and it is not present for the washed nanoparticles. In fact, no peak referring to carboxylic acid or primary amine is observed in the washed sample spectra, indicating the efficiency of the washing procedure with hot acetone in removing the organic layer. In addition, as will be discussed below, the annealed washed nanoparticles present high resistivity, as is expected for $LiFePO_4$. On the other hand, the annealed as-made nanoparticles present high

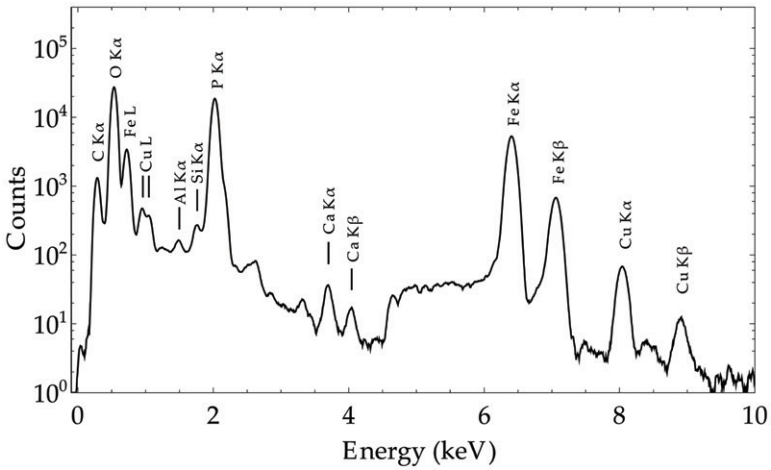

Figure 2. PIXE spectrum of washed $LiCu_xFe_{1-x}PO_4$ ($X = 0.042$) nanoparticles.

conductivity, several orders of magnitude higher than that of the *fat free* washed nanoparticles. This is a consequence of the carbon layer formed by the decomposition of the organic layer at the surface of the particles.

Figure 2 shows the PIXE spectrum with and without the filter of sample $X = 0.042$. The peaks of P, O, Fe and Cu are clearly observed, together with other elements. These elements, namely C, Na and Ca, are contaminants and are probably related to the sample conditioning for this very sensitive measurement and they are present in all the samples. The atomic percentage and its perceptual relative error for each identified element are given in table 1 for all the samples. There is a good relation between the obtained amounts of Fe and P and the expected one for all the samples. We obtained relations between the amounts of Cu and Fe that were equal to 0.042 and 0.001, and these were smaller than the amounts used in the synthesis: 0.06 and 0.005, respectively. Based on these results, we labeled the samples $X = 0$, 0.001 and 0.042. For $X = 0.001$, we remark that the mass used in the synthesis was very small, at the lower limit of our measurement capability, which implies an important error here, and simultaneously the small amount of material used makes it more probable that the Cu content was not so well homogenized in the solution during synthesis.

The crystallinity of the nanoparticles that constitute all the samples was confirmed via XRD patterns with reflections that corresponded to an olivine structure [25], as shown in figure 3. The crystallite size was obtained from the width of the (1 1 1) peak using Scherrer's equation [26], obtaining 34 nm, 41 nm and 39 nm for X =0, 0.001 and 0.042, respectively.

In figure 4(a) we show a representative TEM micrograph with a general view of the nanoparticles of sample $X = 0$. The TEM images evidence the presence of nanoparticles with different shapes, with 67% of them being nearly spherical, 23% having rectangular nanostructures and 10% of them being neither spherical nor rectangular. In figure 4(b) we present a higher magnification micrograph of the same sample, and here an amorphous coating layer of a thickness ranging from 3 to 5 nm is clearly evidenced on the surface of the as-made nanostructures.

Table 1. PIXE spectroscopy results for the three samples: atomic percentage (% at), relative error (%), stoichiometry and Cu/Fe relation.

X	Elem	% at	Rel error %	Stoic	Cu/Fe
	O	63.2	0.2	4.22	0
	P	14.4	0.2	0.96	0
	Fe	12.2	0.2	0.82	0
0	Cu	0.001	142	0	0
	Na	0.5	2.7	—	0
	Ca	0.07	3.1	—	0
	C	9.4	1.1	—	0
	O	65.4	0.2	4.12	0.001
	P	16.2	0.2	1.02	0.001
	Fe	13.7	0.2	0.86	0.001
0.001	Cu	0.006	24.5	0.001	0.001
	Na	0.37	3.7	—	0.001
	Ca	0.07	3.3	—	0.001
	C	4.1	2.0	—	0.001
	O	62.8	0.2	4.11	0.042
	P	15.1	0.2	0.99	0.042
	Fe	13.3	0.2	0.87	0.042
0.042	Cu	0.6	1.5	0.037	0.042
	Na	0.5	3.2	—	0.042
	Ca	0.03	5.7	—	0.042
	C	7.7	1.3	—	0.042

The size distribution histogram for the whole sample is presented in figure 4(c). As our sample is made up of nanostructures of different shapes, the information is broken down into three histograms in figures 4((d)–(f)). With the exception of the spherical-shape case, the '*d*' value used corresponded to the arithmetical average of the dimensions of each nanostructure; for example, in the rectangular shape we measured both sides and considered the mean value for the histogram. The size distribution of the whole sample and the spherical-shape population were fitted with lognormal distributions with mean

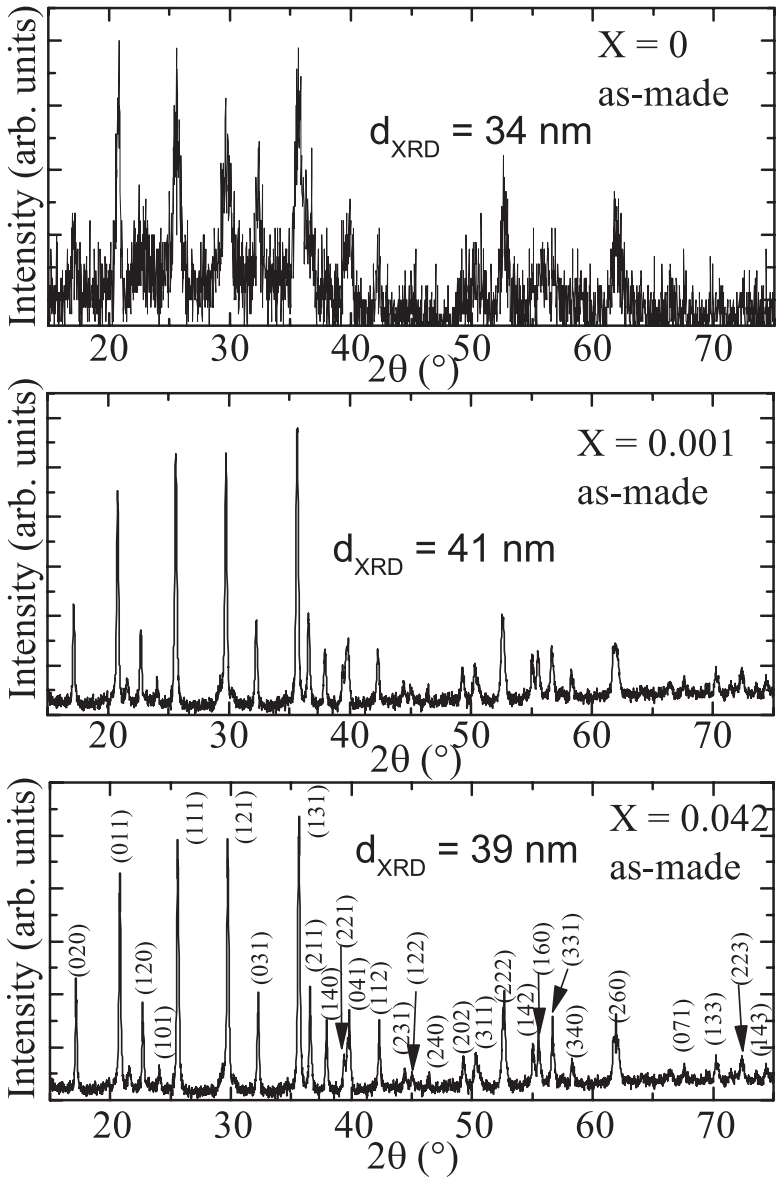

Figure 3. X-rays patterns for as-made $LiCu_xFe_{1-x}PO_4$ nanoparticles ($X = 0$, 0.001 and 0.042). The reflections correspond to the olivine structure [25]. The crystallite size, denoted by d_{XRD} on each panel, was estimated from the (1 1 1) peak using Scherrer's equation [26].

diameters ($\langle d \rangle$) of 27 nm and 25 nm, respectively, and $\sigma = 0.2$ in both cases.

There is an important diversity of results in the literature regarding the shape of $LiCu_xFe_{1-x}PO_4$ nanostructures. Following a similar synthesis method to that presented in this work, Jiang *et al* only obtained rhombohedral nanoparticles [5]. Nevertheless, different shapes of $LiFePO_4$ nanostructures were synthesized by Rangappa *et al* [27] following a supercritical ethanol process in the presence of oleylamine. They observed different morphologies depending on the synthesis temperature: hexagonal nano-plates for 320 °C and nano-rods for 400 °C. It is interesting to note that despite the fact that the synthesis protocol that we followed was not the same as the one followed by Rangappa *et al*, the synthesis temperature was intermediate (380 °C) and we obtained the same mixture of shapes that they observed. Following another protocol, Lim *et al* [28] synthesized $LiFePO_4$ nanostructures using the polyol method. They obtained a variety of nanostructure shapes, depending on the synthesis conditions: orthorhombic, rods, plates and a mixture of these. Interestingly, the authors found that the best electrochemical performance came from an electrode prepared with a mixture of nanostructures of different shapes, arguing that this was a consequence of better nanostructure compaction.

Figure 5 shows representative HRTEM images of spherical-shaped (figure 5(a)), rhombohedral-shaped (figure 5(b)) and rod-shaped (figure 5(c)) nanostructures for $X = 0$. As can be seen in these images, all particles of all shapes present high crystallinity in the whole particle, with well-defined crystalline planes up to the surface of the particle. These planes can be indexed with the crystalline structure of $LiFePO_4$, the same crystalline structure used to index the XRD profiles. In

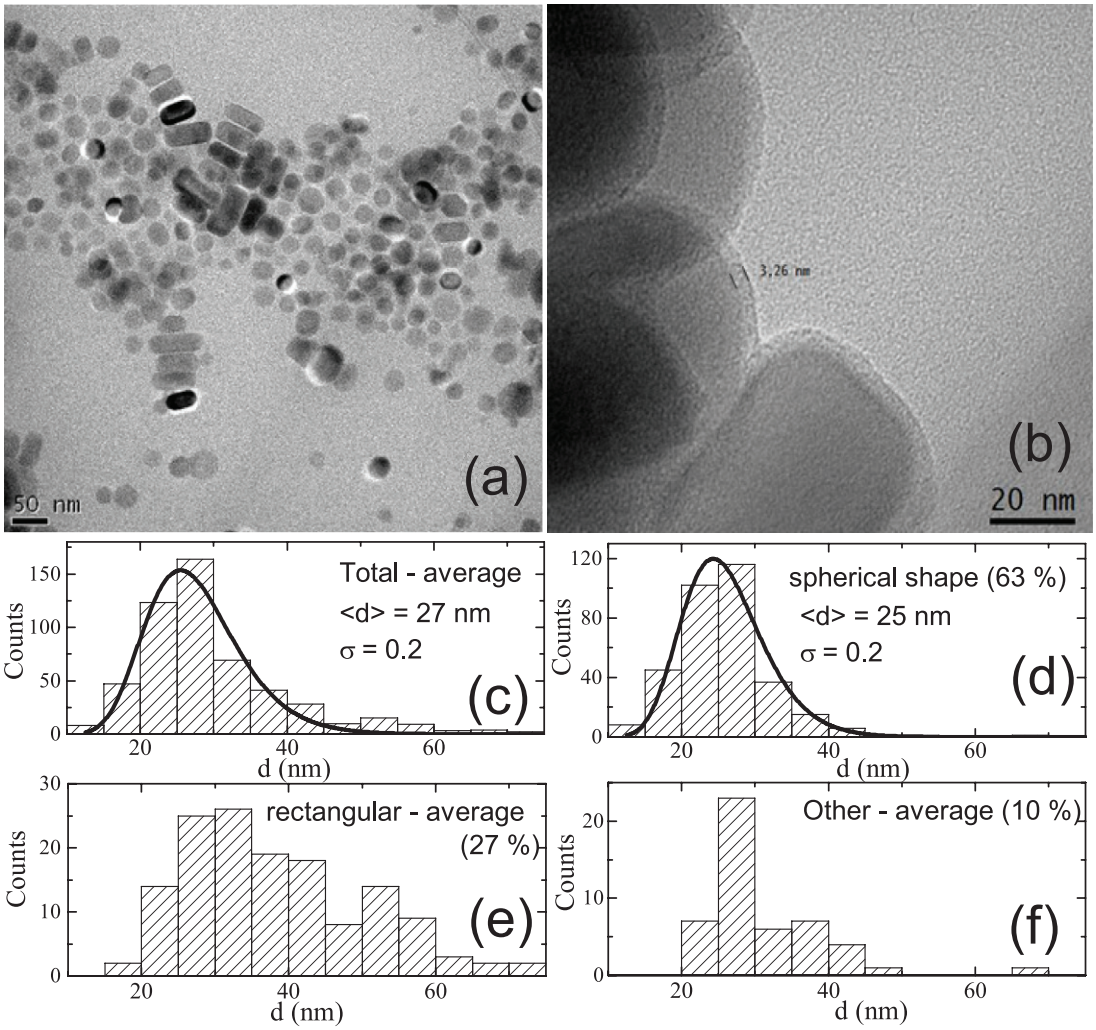

Figure 4. (a) TEM micrograph of the sample $X = 0$. 63% of this sample showed a spherical shape, 27% showed a rectangular shape and 10% showed another shape. (b) HRTEM micrograph of nanoparticles evidencing an organic layer of approximately 3 nm. ((c)–(f)) Histograms of the size distributions of the different nanostructure shapes; see the text for details.

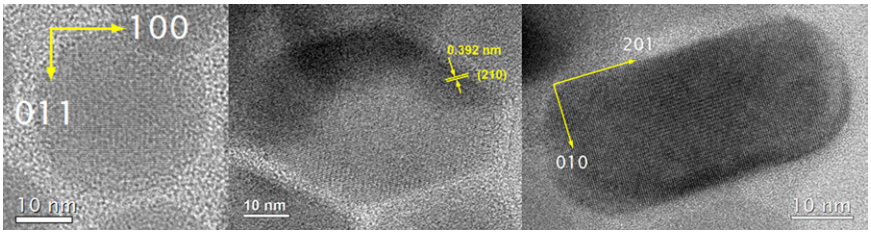

Figure 5. Representative HRTEM images of (a) spherical-shaped, (b) rhombohedral-shaped and (c) rod-shaped nanostructures in sample $X = 0$.

addition, all the particles are single crystals and no evidence of fusion among the particles is observed, which is especially significant for the rod-shaped particles (it is not the percolation of spherical particles). Therefore, the different shapes of the $LiFePO_4$ nanoparticles represent distinct growth directions, and not a percolation of the particles during synthesis. HRTEM images of samples $X = 0.001$ and 0.042 exhibit similar characteristics. These HRTEM results are very interesting, since they clearly evidence that our samples are composed of single crystals with dimensions between 20–40 nm. Thus, the transport properties described below for these nanoscale systems are not associated with poor crystallinity of the system, but with the properties of crystalline $LiFePO_4$ nanoparticles with distinct shapes and the incorporation of the Cu^{2+} ion.

Figure 6(a) presents the IV curves for the three samples ($X = 0$, 0.001 and 0.042), where a linear behavior is observed over the whole range for all the samples. In addition, there is clear evidence of increased resistance as the amount of Cu increases. The DC resistivities (shown in table 2) are obtained from a linear fit of the IV curves. The obtained values are

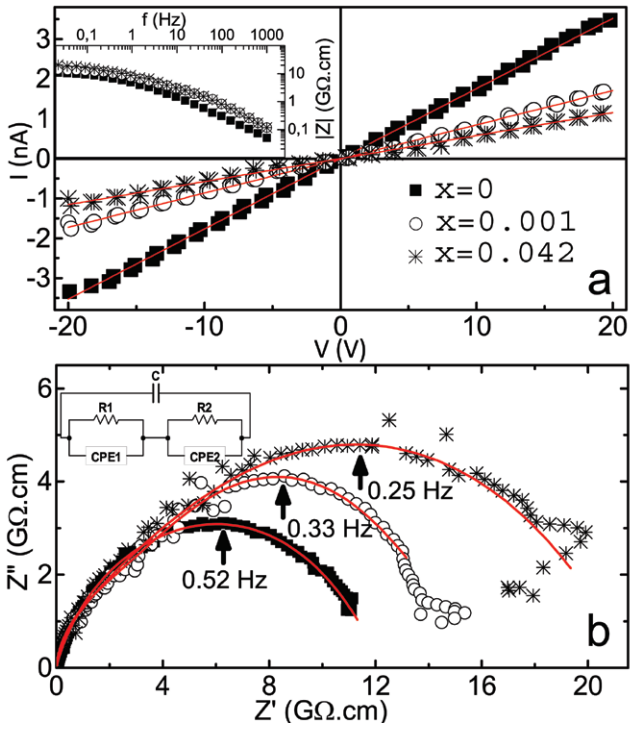

Figure 6. (a) IV curves for all the samples (the solid lines correspond to different linear fits); the inset shows (also for all samples) the absolute value of the impedance as a function of frequency. (b) Nyquist impedance plot of the experimental results and the corresponding fit (solid lines) using the equations of the equivalent circuit shown in the inset; the arrows indicate the frequency of the maximum Z'' (see text for details).

$\rho^{DC} = 10.1$, 10.7 and 13.9 $G\Omega \cdot cm$ for $X = 0$, 0.001 and 0.042, respectively. In all cases, the results are properly normalized by the geometrical factor given by $\frac{\delta}{\mathcal{A}}$, where δ is the thickness of the $LiCu_xFe_{1-x}PO_4$ pellet and $\mathcal{A}$ is the average area of the contacts.

The inset of figure 6(a) presents the amplitude Bode plot for the impedance of all the samples on the (10 mHz–1 kHz) range. Here it is evident that all the samples present a similar response, which can be associated with typical RC-like behavior. In this figure we present the results for frequencies below 1kHz, but the same behavior is observed over the whole frequency range. In these cases the resistive and capacitive contributions are evidenced at low and high frequencies respectively, where the cutoff frequencies are in the 0.1 to 1 Hz range. We can remark that the higher absolute impedance values (reached at low frequencies) are one order of magnitude higher than those previously reported for nanometric $LiFePO_4$ without carbon coating ($\sim 10^9\ \Omega \cdot cm$) by Park *et al* [29].

In figure 6(b) we present the Nyquist impedance plot, where it is possible to highlight the following characteristics. First, the absolute value of the real part of the impedance at the lowest measured frequency range increases with increasing Cu content, which is in perfect agreement with the DC measurements. Second, the frequency of the maximum value of the Z'' decreases with increasing Cu content, as indicated by the arrows. Finally, the Nyquist plot is not exactly semicircular, it manifests an asymmetry at the high frequency range, which indicates the presence of different relaxation mechanisms. These kinds of processes are usually modeled by an equivalent circuit, which is made up of a series of small building blocks associated with different mechanisms. An archetypal case is, for example, charge transport in the presence of a concentration gradient; in this case the asymmetry at high frequencies indicates a transmissive boundary condition [30].

In order to go into the impedance spectroscopy results in depth and correlate them with the electric transport in the $LiCu_xFe_{1-x}PO_4$ nanoparticles, the Nyquist plots of all the samples were modeled using the equations of the frequency response of the equivalent circuit that is sketched in figure 6(b). This equivalent circuit is composed of a capacitor (due to the geometric characteristic of the pellets) connected in parallel with two serial blocks that take into account different relaxation processes [18, 30]. Each one of these building blocks is composed of a resistance R in parallel with a constant phase element (CPE), which has an impedance given by $Z_{CPE} = A(j\omega)^{-n}$, where A and n are free parameters associated with the relaxation time distribution of the system and the frequency $f = \omega/2\pi$. We can remark at this point that the use of two R—CPE blocks was strictly necessary as it was not possible to obtain a good fitting using only one of these blocks.

With the help of EIS Spectrum Analyser software [31] and using the Levenberg–Marquardt algorithm, we fitted the experimental results for the impedance of all the samples. The best fit corresponded to the solid line shown in figure 6(b), and the values of the parameters C, R_1, A_1, n_1, R_2, A_2 and n_2 are given in table 2. The good agreement between the experimental results and the fitting of the equivalent circuits, and the fact that the R and A values found for R–CPE_1 are consistent with those obtained for ionic transport in nanometric amorphous $LiFePO_4$ films [18], strongly suggests that the electric transport is dominated by the ionic contribution in all the samples. We can also remark that—taking into account the recent results reported by Ohmer *et al* [32], which showed velocities for Li^+ diffusion dynamics in the range of tens of nm min^{-1}, and the characteristic time of our experiments—our results evidence the diffusion dynamics. Regarding addition of Cu, we observe that the values obtained for R_1 and CPE_1 systematically manifest the same tendency: as the amount of Cu increases, the impedance value also increases, according to the DC measurements. Despite the fact that there are reports of changes in the electronic structure of $LiFePO_4$ with Cu-doping [33], and results that show improved electrochemical properties for Cu-doped $LiFePO_4$ [34, 35], our experimental results clearly indicate that the addition of Cu worsens the electric transport.

Based on our experimental results for R and R_1, it is possible to estimate the value of the diffusion coefficient (D) related to the Li^+ ion, using the following equation [29, 36]:

$$D = \left(\frac{1}{\rho}\right)\left(\frac{k_B T}{c.(Z.e)^2}\right), \quad (1)$$

Table 2. Resistivity values ρ^{DC} obtained from IV curves. The parameters C, R_1, A_1, n_1, R_2, A_2 and n_2 were obtained by fitting the impedance results with the parameters of the equivalent circuit shown in figure 6(b). The diffusion coefficients D^{DC} and D^{AC} were obtained from ρ, R_1 and equation (1)

Sample X	ρ (G$\Omega \cdot$ cm)	C (pF)	R_1 (G $\Omega \cdot$ cm)	A_1 (G $\Omega \cdot$ cm)	n_1 —	R_2 (G $\Omega \cdot$ cm)	A_2 (G $\Omega \cdot$ cm)	n_2 —	D^{DC} 10^{-13}(cm^{2}s^{-1})	D^{AC} 10^{-13}(cm^{2}s^{-1})
0	10.1	1.6	10	790	0.70	2.2	760	0.61	7.3	7.4
0.001	10.7	1.2	11	630	0.74	4.7	710	0.37	6.9	6.7
0.042	13.9	1.2	17	430	0.60	5.7	510	0.36	5.3	4.3

where c is the volumetric charge concentration and $Z.e$ is the charge of the Li^+. The obtained D^{AC} and D^{DC} values shown in table 2 were calculated using R_1 and ρ, respectively. It is interesting to note that our results give an estimate for the diffusion coefficient that is in-between that of the microcrystalline bulk samples and monocrystals measured in the easy diffusion direction [0 1 0]. In those cases, for $LiFePO_4$ systems, the diffusion coefficients are about 10^{-14}–10^{-15} cm^2 s^{-1} for the microcrystalline bulk [29, 37] and ($\sim 10^{-9}$ cm^2 s^{-1}) for the monocrystal samples measured in the easy diffusion direction [0 1 0] [22].

It is well known from the literature that the incorporation of aliovalent ions improves the electrical properties of $LiFePO_4$ [21], which is assigned to significant changes in the electronic transport mechanism due to the presence of centers with unbalanced charge. The effects of the incorporation of divalent ions on the transport properties of $LiFePO_4$ is a more complicated issue. From the point of view of electronic transport, no change is expected, since the dominant polaron mechanism remains [38]. Regarding the diffusion of Li^+, which is the dominant mechanism for the characteristic time of our transport measurements, the role of the incorporation of divalent ions has not been studied sufficiently, and it is far from being fully understood, especially at the nanometric scale of our particles.

Our results clearly show that the incorporation of Cu into the structure of very crystalline $LiFePO_4$ nanoparticles harms the Li^+ diffusion and consequently the charge transport. This can be assigned to two factors. First, the addition of Cu may lead to a distortion of the crystalline structure that harms the unidirectional diffusion of Li through the (0 1 0) direction. Second, this may be related to some inversion degree in the incorporation of the Cu ions in the crystalline structure, with a partial occupation of Li^+ sites. In this case, it is known that the presence of an ion of higher valency in the Li + site blocks the diffusion and hinders the charge transport by this mechanism [7, 9]. Concerning the distortion in the crystalline structure that is improved by Cu incorporation, Heo *et al* [39] observed a small distortion in copper-doped lithium-rich olivine phosphate powder $Li_{1.05}Fe_{0.997}Cu_{0.003}PO_4$ prepared using a solid-state reaction method at high temperature when compared with the $LiFePO_4$ phase, which led to improved charge–discharge characteristics. In another work on a similar system where the Cu content was verified by x-ray photoelectron spectroscopy (XPS), Lee *et al* [40] observed no significant changes in the XRD profile of the $Li_{1.05}Fe_{0.997}Cu_{0.003}PO_4$, despite the fact that higher cell performance and improved conducting properties were observed for the Cu-substituted olivine phase, and the authors referred to the 'substitution of copper for Fe^{2+} sites' from conductive measurements. Gouveia *et al* [41] observed evidence from Mössbauer and Raman spectroscopy in respect of $LiFePO_4$ containing 3% Cu that the Cu ions were incorporated to the detriment of iron, while a disordered structure was also noted. Jayaprakash *et al* [42] performed local cation environment studies via FTIR on $LiFePO_4$ containing 2% at. Cu ions and the results matched the spectrum expected for the $LiFePO_4$ well, while cyclic voltammograms indicated an excellent reversibility for the Li charge or discharge in the Cu-substituted material. In another way, Upreti *et al* [43] studied the effects of Cu substitution in lithium iron phosphate single crystals formed under hydrothermal conditions and they found that the phase formed with an olivine structure showed partial occupancy of both Li and transition metal sites—$Li_{0.95}[(Fe^{2+})_{0.70}(Fe^{3+})_{0.10} - (Cu^{2+})_{0.15}(Li_{0.05})]PO_4$—while their x-ray and nuclear magnetic resonance (NMR) studies confirmed 5% Li in the Fe site and Fe^{3+} clustering around the Li ions.

4. Conclusions

In summary, using the high-temperature thermal decomposition method, we synthesized highly crystalline $LiCu_xFe_{1-x}PO_4$ ($X = 0$, 0.001 and 0.042) nanoparticles with a diameter of around 40 nm. The amount of Cu was verified for each sample via PIXE spectroscopy. All the samples were highly crystalline with an olivine structure. In terms of morphology, they were composed of nanoparticles that exhibited three different shapes (spheres, rods and rhombus). As-made nanoparticles presented an organic layer at the surface, which was successfully removed through moderate chemical etching, as inferred from FTIR spectroscopy. Electric transport measurements indicated that the systems were highly resistive ($\sim 10^{10}$ $\Omega \cdot$ cm), while the resistance was mainly dominated by Li diffusion. From impedance spectroscopy experiments we estimated a diffusion coefficient for the nanostructured $LiFePO_4$ (in good agreement with previously reported results), and then observed the evolution as a function of the doping level. This paper also shows that the use of Cu as a dopant for highly crystalline $LiFePO_4$ nanoparticles, even in small quantities, degrades the electrical transport properties. This fact, which is mainly due to detrimental effects on the Li diffusion mechanism, should be of considerable interest for the design of $LiFePO_4$-based batteries.

Acknowledgments

The authors are in debt to Dr G A Bocan from the Centro Atómico Bariloche for essential discussions. We also thank the team at the Laboratorio de Caracterización de Materiales for XRD measurements. This work was partially supported by the Agencia Nacional de Promoción Científica y Tecnológica (Argentina) under grants PICT-2011-0752, PICT-2012-1136, PICT-2012-00492 and PICT-2014-2612, by CONICET under grants PIP 490 2012-2014 and PIP-112-2011-00519, and by the Universidad Nacional de Cuyo under the SeCTyP grant 06-C456.

References

[1] Chaudhuri R G and Paria S 2012 Core/shell nanoparticles: classes, properties, synthesis mechanisms, characterization, and applications *Chem. Rev.* **112** 2373–433
[2] Iyer S R and Sastry S M L 1999 Consolidation of nanoparticles—development of a micromechanistic mode *Acta Mater.* **47** 3079–98
[3] Divinski S V and Larikov L N 1997 Diffusion in nanostructured materials *Defect Diffus. Forum* **143–7** 1469–74
[4] Park J, An K, Hwang Y, Park J-G, Noh H-J, Kim J-Y, Park J-H, Hwang N-M and Hyeon T 2004 Ultra-large-scale syntheses of monodisperse nanocrystals *Nat. Mater.* **3** 891–5
[5] Jiang J, Liu W, Chen J and Hou Y 2012 $LiFePO_4$ Nanocrystals: liquid-phase reduction synthesis and their electrochemical performance *Appl. Mater. Interfaces* **4** 3062–8
[6] Padhi A K, Nanjundaswamy N S and Goodenough J B 1997 Phospho-olivines as positive-electrode materials for rechargeable lithium batteries *J. Electrochem. Soc.* **144** 1188–93
[7] Deng S, Wang H, Liu H, Liu J and Yan H 2014 Research progress in improving the rate performance of $LiFePO_4$ cathode materials *Nano-Micro Lett.* **6** 209–26
[8] Zaghib K, Striebel K, Guerfi A, Shim J, Armand M and Gauthier M 2004 $LiFePO_4$-polymer-natural graphite: low cost Li-ion batteries *Electrochim. Acta* **50** 263–70
[9] Wang J and Sun X 2015 Olivine $LiFePO_4$: the remaining challenges for future energy storage *Energy Environ. Sci.* **8** 1110–38
[10] Ma Z, Shao G, Fan Y, Wang G, Song J and Liu T 2014 Tunable morphology synthesis of $LiFePO_4$ nanoparticles as cathode materials for lithium ion batteries *ACS Appl. Mater. Interfaces* **6** 9236–44
[11] Liu Z, Xu B, Xing Y, Li J, Zhang L, Wang L and Fang S 2015 Determination of the relationship between particle size and electrochemical performance of uncoated $LiFePO_4$ materials *J. Nanoparticle Res.* **17** 163
[12] Chung S-Y and Chiang Y-M 2003 Microscale measurements of the electrical conductivity of doped $LiFePO_4$ *Electrochem. Solid State Lett.* **6** A278–81
[13] Song M-K, Park S, Alamgir F M, Cho J and Liu M 2011 Nanostructured electrodes for lithium-ion and lithium-air batteries: the latest developments, challenges, and perspectives *Mater. Sci. Eng.* R **72** 203–252
[14] Ramana C V, Mauger A, Gendron F, Julien C M and Zaghib K 2009 Study of the Li-insertion/extraction process in $LiFePO_4$/$FePO_4$ *J. Power Sources* **187** 555–64
[15] Saiful Islam M, Driscoll D J, Fisher C A J and Slater P R 2005 Atomic-scale investigation of defects, dopants, and lithium transport in the $LiFePO_4$ olivine-type battery material *Chem. Mater.* **17** 5085–92
[16] Delacourt C, Laffont L, Bouchet R, Wurm C, Leriche J-B, Morcrette M, Tarascon J-M and Masquelier C 2005 Toward understanding of electrical limitations (electronic, ionic) in $LiMPO_4$ (M = Fe, Mn) electrode materials *J. Electrochem. Soc.* **152** A913–21
[17] Prosini P P 2011 *Iron Phosphate Materials as Cathodes for Lithium Batteries* (London: Springer) ch 3
[18] Li C-L and Fu Z-W 2007 Kinetics of Li + ion diffusion into $FePO_4$ and FePON thin films characterized by AC impedance spectroscopy *J. Electrochem. Soc.* **154** A784–91
[19] Wang J and Sun X 2012 Understanding and recent development of carbon coating on $LiFePO_4$ cathode materials for lithium-ion batteries *Energy Environ. Sci.* **5** 5163–85
[20] Chung S Y, Bloking J T and Chiang Y-M 2002 Electronically conductive phospho-olivines as lithium storage electrodes *Nat. Mater.* **1** 123–8
[21] Meethong N, Kao Y-H, Speakman S A and Chiang Y-M 2009 Aliovalent substitutions in olivine lithium iron phosphate and impact on structure and properties *Adv. Funct. Mater.* **19** 1060–70
[22] Amin R, Balayam P and Maier J 2007 Anisotropy of electronic and ionic transport in $LiFePO_4$ single crystals *Electrochem. Solid-State Lett.* **10** A13–6
[23] Johansson S A E, Campbell J L and Malmqvist K G 1995 *Particle-Induced X-ray Emission Spectrometry (PIXE)* (Hoboken, NJ: Wiley)
[24] Barsoukov E 2005 Electrochemical power sources *Impedance Spectroscopy: Theory, Experiment, and Applications* ed E Barsoukov and J R Macdonald (Hoboken, NJ: Wiley) pp 430–68
[25] Yakubovich O V, Simonov M A and Belov N V 1977 The crystal structure of a synthetic triphylite LiFe[PO_4] *Sov. Phys.—Dokl.* **22** 347
[26] Cullity B D 1978 *Elements of X-ray Diffraction* (Reading, MA: Addison-Wesley)
[27] Rangappa D, Sone K, Ichihara M, Kudob T and Honma I 2010 Rapid one-pot synthesis of $LiMPO_4$ (M = Fe, Mn) colloidal nanocrystals by supercritical ethanol process *Chem. Commun.* **46** 7548–50
[28] Lim J, Mathew V, Kim K, Moon J and Kim J 2011 One-pot synthesis of multi-morphous $LiFePO_4$ nanoparticles in polyol medium *J. Electrochem. Soc.* **158** A736–40
[29] Park M, Zhang X, Chung M, Less G B and Sastrya A M 2010 A review of conduction phenomena in Li-ion batteries *J. Power Sources* **195** 7904–29
[30] Raistrick I D, Franceschetti D R and Macdonald J R 2005 Chapter 2: Theory *Impedance Spectroscopy: Theory, Experiment, and Applications* 2nd edn, ed E Barsoukov and J R Macdonald (Hoboken, NJ: Wiley)
[31] Bondarenko A S and Ragoisha G A *EIS Spectrum Analyser* www.abc.chemistry.bsu.by/vi/analyser/
[32] Ohmer N, Fenk B, Samuelis D, Chen C-C, Maier J, Weigand M, Goering E and Schutz G 2015 Phase evolution in single-crystalline $LiFePO_4$ followed by *in situ* scanning x-ray microscopy of a micrometre-sized battery *Nat. Commun.* **6** 6045–9
[33] Abbatea M, Lala S M, Montoro L A, Rosolen J M 2005 Ti-, Al-, and Cu-doping induced gap states in $LiFePO_4$ *Electrochem. Solid-State Lett.* **8** A288–90
[34] Yang R, Song X, Zhao M and Wang F 2009 Characteristics of $Li_{0.98}Cu_{0.01}FePO_4$ prepared from improved co-precipitation *J. Alloys Compd.* **468** 365–9
[35] Yi T-F, Li X-Y, Liu H, Shu J, Zhu Y-R and Zhu R-S 2012 Recent developments in the doping and surface modification of $LiFePO_4$ as cathode material for power lithium ion battery *Ionics* **18** 529–39
[36] Kofstad P and Norby T 2007 *Defects and Transport in Crystalline Solids* 1st edn (Oslo: University of Oslo) ch 6

[37] Dathar G K P, Sheppard D, Stevenson K J and Henkelman G 2011 Calculations of Li-ion diffusion in olivine phosphates *Chem. Mater.* **23** 4032–7
[38] Hoang K and Johannes M 2011 Tailoring native defects in $LiFePO_4$: insights from first-principles calculations *Chem. Mater.* **23** 3003–13
[39] Heo J B, Lee S B, Cho S H, Kim J, Park S H and Lee Y S 2009 Synthesis and electrochemical characterizations of dual doped $Li_{1.05}Fe_{0.997}Cu_{0.003}PO_4$ *Mater. Lett.* **63** 581–3
[40] Lee S B, Cho S H, Heo J B, Aravindana V, Kim H S and Lee Y S 2009 Copper-substituted, lithium rich iron phosphate as cathode material for lithium secondary batteries *J. Alloys Compd.* **488** 380–5
[41] Gouveia D X, Lemos V, Paiva J A C, Souza Filho A G, Mendes Filho J, Lala S M, Montoro L A and Rosolen J M 2005 Spectroscopic studies of $LixFePO_4$ and $Li_xM_{0.03}Fe_{0.97}PO_4$ (M = Cr,Cu,Al,Ti) *Phys. Rev.* B **72** 024105
[42] Jayaprakash N, Kalaiselvi N and Periasamy P 2008 Synthesis and characterization of $LiM_XFe_{1-X}PO_4$ (M = Cu, Sn; $X = 0.02$) cathodes—a study on the effect of cation substitution in $LiFePO_4$ material *Int. J. Electrochem. SC* **3** 476–88
[43] Upreti S *et al* 2012 Crystal structure, physical properties, and electrochemistry of copper substituted $LiFePO_4$ single crystals *Chem. Mater.* **23** 166–73